Approximate solution to the bidomain equations for defibrillation problems

Salil G. Patel and Bradley J. Roth*
Department of Physics, Oakland University, Rochester, Michigan 48309, USA
(Received 6 August 2004; published 23 February 2005)

The bidomain model can be used for calculating the electrical potential in the heart during defibrillation. However, this model consists of a coupled system of two partial differential equations that are, in general, difficult and time consuming to solve. In this paper, we present an approximate, iterative method of solving the bidomain equations. After working out the general method, we apply it to four problems: (i) a cylindrical strand in a uniform electric field, (ii) a nonuniform electric field applied to tissue with straight fibers, (iii) a spherical heart in a uniform electric field, and (iv) a two-dimensional sheet of cardiac tissue with curving fibers. Finally, we analyze the general case of three dimensions.

DOI: 10.1103/PhysRevE.71.021908 PACS number(s): 87.18.−h, 87.10.+e

I. INTRODUCTION

When the heart goes into ventricular fibrillation, the only effective treatment is to apply a large electrical shock: defibrillation. The design of defibrillators would be simplified if we could easily calculate the voltages produced in the heart during the shock. The best model for performing such a calculation is the bidomain model [1], which is a two- or three-dimensional cable model that accounts for the flow of current through the intracellular and extracellular spaces of cardiac tissue. It is a continuum model, so the macroscopic electrical properties of the tissue are spatial averages over many cells. In general, cardiac tissue is anisotropic (different electrical properties in different directions), and the bidomain model takes this anisotropy into account. In particular, many of the interesting results of the bidomain model arise when the intracellular and extracellular spaces have different degrees of anisotropy (unequal anisotropy ratios). Researchers often use the bidomain model to study electrical stimulation of the heart [2–7]. However, the bidomain model consists of a coupled system of two partial differential equations that are, in general, difficult and time consuming to solve. Much software that has been developed for solving general boundary value problems such as Laplace's equation cannot be used to solve the bidomain equations.

In this paper, we present an approximate, iterative method for solving the bidomain equations. This method has two useful attributes: (i) numerical simulations can be performed using commercial software designed to solve general boundary value problems, and (ii) often analytical solutions can be found, even for unequal anisotropy ratios, that provide more insight into the physical behavior than do numerical computations alone. After working out the general method, we access its accuracy and utility by applying it to several problems that have been studied previously.

II. GENERAL PROBLEM

The bidomain equations governing the intracellular and extracellular potentials, V_i and V_e, in steady-state and assuming a passive membrane, are

$$\nabla \cdot (\tilde{g}_i \nabla V_i) = \beta G_m (V_i - V_e), \tag{1}$$

$$\nabla \cdot (\tilde{g}_e \nabla V_e) = -\beta G_m (V_i - V_e), \tag{2}$$

where $\tilde{g}_i$ and $\tilde{g}_e$ are the intracellular (i) and extracellular (e) conductivity tensors, β is the ratio of membrane area to tissue volume, and G_m is the membrane conductivity per unit area. The quantities $\tilde{g}_i$ and $\tilde{g}_e$ are tensors because the electrical properties of cardiac tissue are anisotropic: they are different in the direction parallel to the fibers (longitudinal L) than in the direction perpendicular to them (transverse T). The intracellular conductivity tensor depends on the intracellular conductivity in the longitudinal direction g_{iL} and in the transverse direction g_{iT}, and on the fiber angle, which may vary throughout the tissue. Similarly, the extracellular conductivity depends on g_{eL}, g_{eT}, and the fiber angle.

The bidomain equations [Eqs. (1) and (2)] are coupled, making them difficult to solve. Our goal is to uncouple them. Start with a change of variable

$$V_m = V_i - V_e, \quad \psi = \frac{\alpha}{1+\alpha}\left(V_i + \frac{1}{\alpha} V_e\right), \tag{3}$$

with the inverse transformation

$$V_i = \psi + \frac{1}{1+\alpha} V_m, \qquad V_e = \psi - \frac{\alpha}{1+\alpha} V_m, \tag{4}$$

where $\alpha = g_{iT}/g_{eT}$, V_m is the transmembrane potential, and ψ is an auxiliary potential. (The definitions of α and ψ are slightly different than used previously [2–4].) If we write the bidomain equations in terms of these new potentials and then add Eqs. (1) and (2), we find

$$\nabla \cdot (\tilde{g}_i + \tilde{g}_e) \nabla \psi = -\frac{1}{1+\alpha} \nabla \cdot (\tilde{g}_i - \alpha \tilde{g}_e) \nabla V_m. \tag{5}$$

Similarly, if we multiply Eq. (2) by α and then subtract the product from Eq. (1), we get

*Author to whom correspondence should be addressed. Electronic mail: roth@oakland.edu

$$\nabla \cdot \left(\tilde{g}_i \frac{1}{\alpha} + \alpha \tilde{g}_e \right) \nabla V_m - \frac{(1+\alpha)^2}{\alpha} \beta G_m V_m = -\frac{1+\alpha}{\alpha} \nabla \cdot (\tilde{g}_i - \alpha \tilde{g}_e) \nabla \psi. \quad (6)$$

An important limiting case of the bidomain equations is when the tissue has "equal anisotropy ratios" ($g_{iL}/g_{iT} = g_{eL}/g_{eT}$). In this case the conductivity tensors are proportional, $\tilde{g}_i = \alpha \tilde{g}_e$, so the right-hand sides of Eqs. (5) and (6) are zero and the bidomain equations uncouple. This suggests an iterative approach to solving the full bidomain equations:

$$\nabla \cdot (\tilde{g}_i + \tilde{g}_e) \nabla \psi^n = -\frac{1}{1+\alpha} \nabla \cdot (\tilde{g}_i - \alpha \tilde{g}_e) \nabla V_m^{n-1}, \quad (7)$$

$$\nabla \cdot \left(\tilde{g}_i \frac{1}{\alpha} + \alpha \tilde{g}_e \right) \nabla V_m^n - \frac{(1+\alpha)^2}{\alpha} \beta G_m V_m^n = -\frac{1+\alpha}{\alpha} \nabla \cdot (\tilde{g}_i - \alpha \tilde{g}_e) \nabla \psi^{n-1}, \quad (8)$$

where during the nth iteration we solve the bidomain equations for V_m^n and ψ^n using the previous iteration in the source terms on the right-hand sides. This iterative scheme starts with the solution to the uncoupled bidomain equations for equal anisotropy ratios,

$$\nabla \cdot (\tilde{g}_i + \tilde{g}_e) \nabla \psi^0 = 0, \quad (9)$$

$$\nabla \cdot \left(\tilde{g}_i \frac{1}{\alpha} + \alpha \tilde{g}_e \right) \nabla V_m^0 - \frac{(1+\alpha)^2}{\alpha} \beta G_m V_m^0 = 0. \quad (10)$$

In order to completely describe the bidomain problem, we need to account for the surrounding bath, of conductivity g_b, and the tissue-bath boundary conditions. We assume that the bath potential V_b obeys Laplace's equation,

$$\nabla^2 V_b = 0. \quad (11)$$

(A minor generalization would allow us to describe an anisotropic, inhomogeneous bath, but we will not consider that case in this study.) At the tissue-bath boundary, the boundary conditions are (i) the extracellular potential is equal to the bath potential, (ii) the normal component of the extracellular current density is equal to the normal component of the bath current density, and (iii) the normal component of the intracellular current density is zero [8,9]. In almost all cases of interest, the cardiac fibers at the tissue surface lie parallel to the surface. We will assume that this is the case throughout the rest of our analysis. Mathematically, we can write the boundary conditions as

$$V_e = V_b, \quad (12)$$

$$g_{eT} \frac{\partial V_e}{\partial n} = g_b \frac{\partial V_b}{\partial n}, \quad (13)$$

$$g_{iT} \frac{\partial V_i}{\partial n} = 0, \quad (14)$$

where n is the direction perpendicular to the surface, going into the tissue. Now we need to express these boundary conditions in terms of the variables V_m and ψ. If we use Eq. (4) and some algebra, the boundary conditions become

$$\psi - \frac{\alpha}{1+\alpha} V_m = V_b, \quad (15)$$

$$g_{eT}(1+\alpha) \frac{\partial \psi}{\partial n} = g_b \frac{\partial V_b}{\partial n}, \quad (16)$$

$$\frac{\partial V_m}{\partial n} = -(1+\alpha) \frac{\partial \psi}{\partial n}. \quad (17)$$

Finally, the outer edge of the bath has boundary conditions. For instance, V_b may be specified on the boundary, the boundary may be sealed ($\partial V_b / \partial n = 0$), or we may assume that far from the heart the electric field is uniform. These boundary conditions depend on the electrode geometry used during defibrillation.

Let us now summarize our results, at least for the case of equal anisotropy ratios (the first step of our iteration scheme). Equations (9)–(11), with the boundary conditions in Eqs. (15)–(17) and additional boundary conditions at the outer surface of the bath, govern ψ, V_m, and V_b. The equations for V_m and ψ are not completely uncoupled, even for equal anisotropy ratios, because of the boundary conditions. Although Eq. (9) does not contain V_m, the boundary condition in Eq. (15) does, so we still have not achieved our main goal: uncoupled problems for V_m and ψ.

To make further progress, we must make an assumption. Equation (10) implies that there are no sources of V_m^0 within the tissue (sources arising from fiber curvature, for example, require unequal anisotropy ratios; we will deal with them later). The only source of V_m^0 is from the boundary. Intuitively, this is no surprise; we expect the tissue to be polarized at the boundary. Let us assume that V_m^0 falls off exponentially with depth into the tissue,

$$V_m^0 = A e^{-n/\lambda}, \quad (18)$$

where A can vary in the plane of the surface, n measures depth below the surface in the normal direction, and λ is the length constant in the direction perpendicular to the fibers,

$$\lambda = \sqrt{\frac{g_{iT} g_{eT}}{(g_{iT} + g_{eT}) \beta G_m}}. \quad (19)$$

This result is exact for the one-dimensional case [8]. It should be approximately correct as long as V_m^0 changes in the directions parallel to the tissue surface over distances that are much larger than λ (about 0.2 mm [5]). We can substitute this expression for V_m^0 into the boundary conditions in Eqs. (15)–(17) and simplify. We find two boundary conditions for ψ^0 and V_b,

$$\psi^0 - \lambda \alpha \frac{\partial \psi^0}{\partial n} = V_b, \quad (20)$$

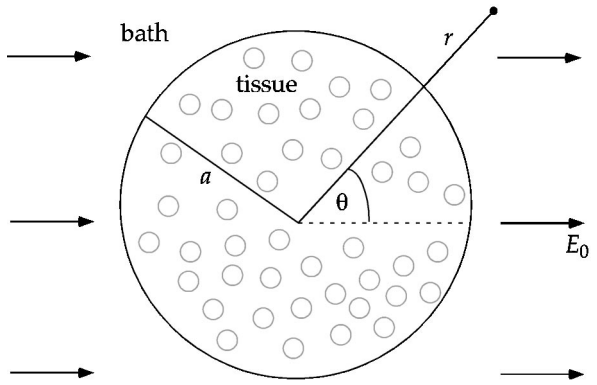

FIG. 1. A cylindrical strand of cardiac tissue of radius a perfused by a bath. A uniform electric field of strength E_0 is applied perpendicular to the strand.

$$g_T \frac{\partial \psi^0}{\partial n} = g_b \frac{\partial V_b}{\partial n}, \tag{21}$$

where $g_T = g_{iT} + g_{eT}$. The third condition gives

$$A = \lambda(1+\alpha)\frac{\partial \psi^0}{\partial n}. \tag{22}$$

We have now accomplished our goal of uncoupling the bidomain equations. Equations (9) and (11) are solved for ψ^0 and V_b, using the boundary conditions in Eqs. (20) and (21). Once ψ^0 is known, V_{m0} is specified by Eqs. (18) and (22). Higher order terms can be calculated as needed. To determine the utility of this method, we consider four examples.

III. EXAMPLE 1: CYLINDRICAL STRAND IN A UNIFORM FIELD

Consider a cylindrical strand of cardiac tissue, of radius a, in an electric field E_0 perpendicular to the strand (Fig. 1). The fibers lie along the length of the strand (z); we ignore end effects so the potentials are independent of z, and the conductivities in both the x and y directions are $g_{ix} = g_{iy} = g_{iT}$, $g_{ex} = g_{ey} = g_{eT}$. Because there are no potential gradients in the fiber direction, the tissue in this example behaves as if it were isotropic and the zeroth order term in the iteration scheme is the full solution (so, we drop the superscripts for this example). The main reason we examine this problem is to investigate the implications of assuming an exponential decay of the transmembrane potential.

Equations (9) and (11), written in cylindrical coordinates (r, θ), simplify to

$$\frac{1}{r}\frac{\partial}{\partial r}\left(r\frac{\partial \psi}{\partial r}\right) + \frac{1}{r^2}\frac{\partial^2 \psi}{\partial \theta^2} = 0, \tag{23}$$

$$\frac{1}{r}\frac{\partial}{\partial r}\left(r\frac{\partial V_b}{\partial r}\right) + \frac{1}{r^2}\frac{\partial^2 V_b}{\partial \theta^2} = 0. \tag{24}$$

The electric field in the bath far from the strand is uniform and in the x direction, so as r becomes large V_b reduces to $-E_0 r \cos\theta$. General solutions to Eqs. (23) and (24) can be written as

$$\psi = B\, r \cos\theta, \tag{25}$$

$$V_b = -E_0 r \cos\theta + \frac{C}{r}\cos\theta, \tag{26}$$

where B and C are unknown constants to be determined by the boundary conditions. As before, we assume V_m falls exponentially with depth below the surface [Eq. (18)]

$$V_m = A \cos\theta\, e^{-(a-r)/\lambda}. \tag{27}$$

Applying the conditions in Eqs. (20)–(22) and solving for A, B, and C gives

$$A = \lambda E_0 \left[\frac{2\frac{g_b}{g_T}(1+\alpha)}{1+\frac{g_b}{g_T}\left(1+\frac{\lambda}{a}\alpha\right)}\right], \quad B = -E_0\left[\frac{2\frac{g_b}{g_T}}{1+\frac{g_b}{g_T}\left(1+\frac{\lambda}{a}\alpha\right)}\right],$$

$$C = E_0 a^2 \left[\frac{1-\frac{g_b}{g_T}\left(1+\frac{\lambda}{a}\alpha\right)}{1+\frac{g_b}{g_T}\left(1+\frac{\lambda}{a}\alpha\right)}\right]. \tag{28}$$

These expressions contain the factor $(1+\lambda\alpha/a)$. Our assumption that V_m falls exponentially only applies if the surface appears "flat"; the surface curves little over distances on the order of a length constant. For this problem, a smooth surface is equivalent to saying $a \gg \lambda$. Furthermore, α is typically on the order of 0.25 [2]. Thus $(1+\lambda\alpha/a)$ is approximately equal to 1. Throughout the remainder of this paper, we will assume the surface is flat, which is equivalent to taking the boundary condition in Eq. (20) to be

$$\psi^0 = V_b. \tag{29}$$

With this approximation, A, B, and C become

$$A = E_0\lambda\left[\frac{2\frac{g_b}{g_T}(1+\alpha)}{1+\frac{g_b}{g_T}}\right], \quad B = -E_0\left[\frac{2\frac{g_b}{g_T}}{1+\frac{g_b}{g_T}}\right],$$

$$C = E_0 a^2\left[\frac{1-\frac{g_b}{g_T}}{1+\frac{g_b}{g_T}}\right]. \tag{30}$$

This example is useful because an exact analytical solution to the full bidomain equations exists. The transmembrane potential is

$$V_m = \frac{1+\alpha}{\alpha} 2aE_0 \frac{I_1\left(\frac{r}{\lambda}\right)}{I_1\left(\frac{a}{\lambda}\right)} \frac{1}{1+\frac{a}{\alpha\lambda}\left(1+\frac{g_T}{g_b}\right)\frac{I_1'(a/\lambda)}{I_1(a/\lambda)}}, \tag{31}$$

where I_1 is the modified Bessel function of the first kind and I_1' is its derivative. Figure 2 compares the approximate [Eqs.

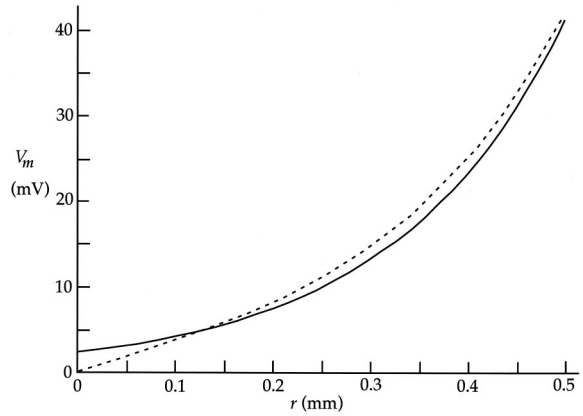

FIG. 2. The approximate analytical (solid) and exact numerical (dashed) transmembrane potentials plotted versus radial distance for a cylindrical strand of cardiac tissue. $a=0.5$ mm, $\alpha=0.25$, $\lambda=0.174$ mm, $g_T=0.0931$ S/m, $g_b=2$ S/m, and $E_0=100$ V/m.

(27) and (30)] and exact [Eq. (31)] values for V_m, for a 0.5 -mm-radius strand (about the size of a papillary muscle). The agreement is good, considering how thin the strand is. Only at the strand center do the exact and approximate solutions deviate significantly.

IV. EXAMPLE 2: NONUNIFORM FIELD APPLIED TO TISSUE WITH STRAIGHT FIBERS

In the previous example, the solution for equal anisotropy ratios corresponded to the full solution to the bidomain equations. In most cases, this is not true. Cardiac tissue does not have equal anisotropy ratios [2]. When fibers curve [4,6] or when the applied electric field is not uniform [7], unequal anisotropy ratios results in polarization far from the tissue boundary. If the model is to be useful, we must account for these effects by examining additional terms in our iterative scheme.

Consider a problem analyzed by Otani [7]: A nonuniform potential exists on the surface of a slab of cardiac tissue having unequal anisotropy ratios. The fibers are straight and in the x direction (Fig. 3). The y direction points into the tissue, and the potential is independent of z. We first solve Eq. (9) for ψ^0,

$$g_L\frac{\partial^2\psi^0}{\partial x^2}+g_T\frac{\partial^2\psi^0}{\partial y^2}=0, \tag{32}$$

where $g_L=g_{iL}+g_{eL}$. Like Otani, we assume that the potential on the surface ($y=0$) varies sinusoidally

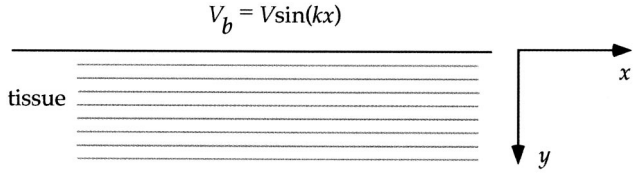

FIG. 3. A two-dimensional slab of cardiac tissue with the fibers aligned along the x direction.

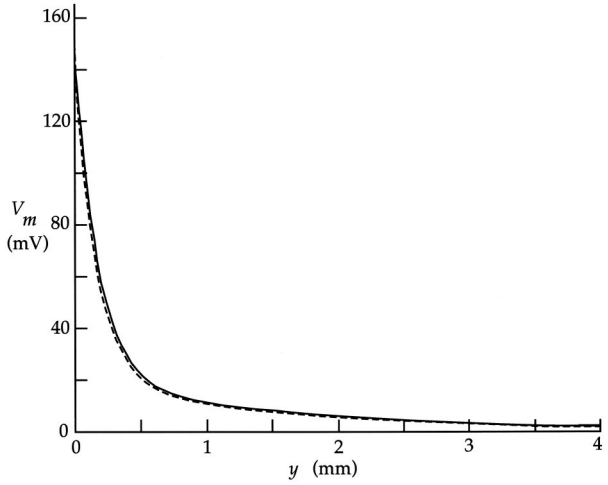

FIG. 4. The approximate analytical (solid) and exact numerical (dashed) transmembrane potentials plotted versus depth below the surface of a slab of cardiac tissue. $\alpha=0.25$, $e=0.75$, $\lambda=0.174$ mm, $g_T=0.0931$ S/m, $g_L=0.3726$ S/m, $V=1$ V, and $k=0.3$ mm^{-1}. The numerical solution used a space step of 0.0125 mm and a slab thickness of 20 mm.

$$V_b = V\sin(kx). \tag{33}$$

The solution of Eq. (32) for ψ^0 is

$$\psi^0 = Be^{-\sqrt{(g_L/g_T)}ky}\sin(kx). \tag{34}$$

As before, we assume that the transmembrane potential falls exponentially with depth into the tissue,

$$V_m^0 = A\sin(kx)e^{-y/\lambda}. \tag{35}$$

The boundary condition in Eq. (29) implies that $B=V$, and Eq. (22) implies that $A=-V\lambda k\sqrt{g_L/g_T}(1+\alpha)$.

The next step is to look at the first order term for the transmembrane potential, which will include the effects of unequal anisotropy ratios. The equation for V_m^1 [Eq. (8)] written in terms of α, g_L, g_T, and $e=1-(g_{eL}/g_{eT})/(g_{iL}/g_{iT})$, is

$$\frac{g_L}{g_T}\left(\frac{1+\alpha-\alpha e}{1+\alpha-e}\right)\frac{\partial^2V_m^1}{\partial x^2}+\frac{\partial^2V_m^1}{\partial y^2}-\frac{1}{\lambda^2}V_m^1 = -\frac{g_L}{g_T}e\left(\frac{1+\alpha}{1+\alpha-e}\right)\frac{\partial^2\psi^0}{\partial x^2}. \tag{36}$$

Throughout this analysis, we assume that the potential ψ^0 changes slowly over distances on the order of a length constant. In that case, the second derivative terms on the left-hand side of Eq. (36) are small, and V_m^1 becomes

$$V_m^1 = -Vk^2\lambda^2\frac{g_L}{g_T}e\left(\frac{1+\alpha}{1+\alpha-e}\right)e^{-\sqrt{(g_L/g_T)}ky}\sin(kx). \tag{37}$$

Because $k\lambda \ll 1$, the V_m^1 term decays more slowly in depth than the V_m^0 term. More than several length constants into the tissue, the V_m^1 term dominates.

Figure 4 compares our approximate analytical solution [Eqs. (35) and (37)] with a numerical solution of the full bidomain equations [Eqs. (5) and (6)], for $k=0.3$ mm^{-1} (cor-

responding to a wavelength of 21 mm). To solve the problem numerically, we used a successive overrelaxation scheme. The transmembrane potential has a rapid decay near the tissue surface, and a slower decay deeper in the tissue. The agreement between the two solutions is excellent. Inherent in our calculation is the assumption that all length scales are much longer than the length constant. Thus we expect our analysis to be valid only when $k\lambda \ll 1$.

V. EXAMPLE 3: SPHERICAL HEART

Trayanova *et al.* [6] studied a spherical heart in order to gain insight into defibrillation. The model consists of a shell of cardiac tissue surrounding a blood cavity and surrounded by a conducting bath (Fig. 5). The inner and outer radii of the shell are b and a, and the conductivity of the blood and bath are g_b and g_o. A uniform electric field of strength E_0 is applied in the z direction. The fibers are in the θ direction, and azimuthal symmetry implies that the potential is independent of the angle ϕ. In spherical coordinates (r, θ, ϕ), Eq. (9) for ψ^0 is

$$g_T \frac{1}{r}\frac{\partial^2}{\partial r^2}(r\psi^0) + g_L \frac{1}{r^2}\frac{1}{\sin\theta}\frac{\partial}{\partial\theta}\left(\sin\theta\frac{\partial\psi^0}{\partial\theta}\right) = 0, \tag{38}$$

and V_o and V_b obey Laplace's equation. Far from the sphere, $V_o = -E_0 r\cos\theta$. General solutions for the potentials are

$$\psi^0 = (Cr^{\nu_1} + Dr^{\nu_2})\cos\theta, \tag{39}$$

$$V_b = Br\cos\theta, \tag{40}$$

$$V_o = -E_0 r\cos\theta + \frac{F}{r^2}\cos\theta, \tag{41}$$

where

$$\nu_{1,2} = -\frac{1}{2} \pm \sqrt{2\frac{g_L}{g_T} + \frac{1}{4}}. \tag{42}$$

Constants B, C, D, and F are determined by applying the boundary conditions $\psi^0 = V_b$ and $g_T(\partial\psi^0/\partial r) = g_b(\partial V_b/\partial r)$ at $r=b$ and $\psi^0 = V_o$ and $g_T(\partial\psi^0/\partial r) = g_o(\partial V_o/\partial r)$ at $r=a$,

$$B = -E_0\left[\frac{3\left(\frac{g_T}{g_b}\right)\left(\frac{a}{b}\right)^{1-\nu_2}(\nu_1-\nu_2)}{\left(1-\frac{g_T}{g_b}\nu_1\right)\left(2+\frac{g_T}{g_o}\nu_2\right)-\left(\frac{a}{b}\right)^{\nu_1-\nu_2}\left(1-\frac{g_T}{g_b}\nu_2\right)\left(2+\frac{g_T}{g_o}\nu_1\right)}\right], \tag{43}$$

$$C = E_0 a^{1-\nu_1}\left[\frac{3\left(\frac{a}{b}\right)^{\nu_1-\nu_2}\left(1-\frac{g_T}{g_b}\nu_2\right)}{\left(1-\frac{g_T}{g_b}\nu_1\right)\left(2+\frac{g_T}{g_o}\nu_2\right)-\left(\frac{a}{b}\right)^{\nu_1-\nu_2}\left(1-\frac{g_T}{g_b}\nu_2\right)\left(2+\frac{g_T}{g_o}\nu_1\right)}\right], \tag{44}$$

$$D = -E_0 a^{1-\nu_2}\left[\frac{3\left(1-\frac{g_T}{g_b}\nu_1\right)}{\left(1-\frac{g_T}{g_b}\nu_1\right)\left(2+\frac{g_T}{g_o}\nu_2\right)-\left(\frac{a}{b}\right)^{\nu_1-\nu_2}\left(1-\frac{g_T}{g_b}\nu_2\right)\left(2+\frac{g_T}{g_o}\nu_1\right)}\right], \tag{45}$$

$$F = -E_0 a^3\left[\frac{\left(1-\frac{g_T}{g_b}\nu_1\right)\left(1-\frac{g_T}{g_o}\nu_2\right)-\left(\frac{a}{b}\right)^{\nu_1-\nu_2}\left(1-\frac{g_T}{g_b}\nu_2\right)\left(1-\frac{g_T}{g_o}\nu_1\right)}{\left(1-\frac{g_T}{g_b}\nu_1\right)\left(2+\frac{g_T}{g_o}\nu_2\right)-\left(\frac{a}{b}\right)^{\nu_1-\nu_2}\left(1-\frac{g_T}{g_b}\nu_2\right)\left(2+\frac{g_T}{g_o}\nu_1\right)}\right], \tag{46}$$

Once again, V_m^0 falls exponentially with depth below the tissue surface. The effect of unequal anisotropy ratios is included in V_m^1. If the potentials vary slowly over distances on the order of a length constant, then we can ignore the terms containing second derivatives and find

$$V_m^1 = -2\frac{\lambda^2}{r^2}\frac{g_L}{g_T}e\left(\frac{1+\alpha}{1+\alpha-e}\right)(Cr^{\nu_1} + Dr^{\nu_2})\cos\theta. \tag{47}$$

Figure 6 compares our approximate analytical solution with a numerical solution of the full bidomain equations. The transmembrane potential reaches about 80 mV at the tissue surface, and decays within a few length constants of the surface to a relatively constant value between 1 and 2 mV within the tissue bulk. Qualitatively, this behavior is consistent with Trayanova *et al.*'s calculation [6], and the quantitative differences are caused by the different parameters' val-

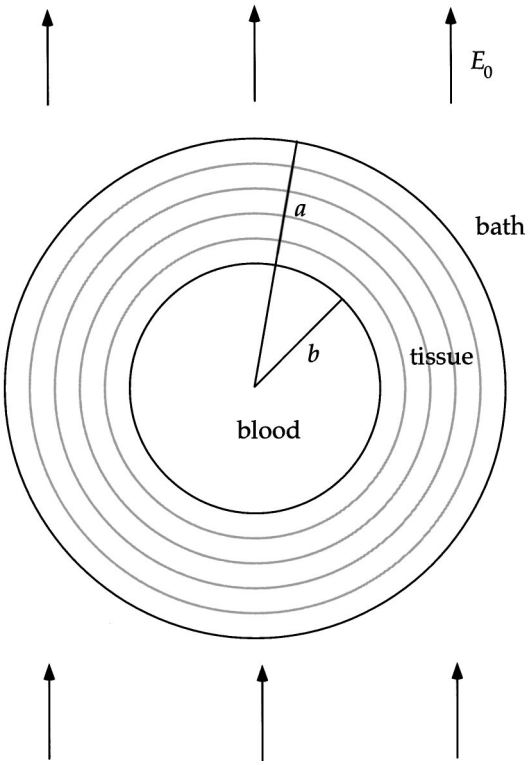

FIG. 5. A spherical shell of cardiac tissue surrounding a blood cavity and surrounded by an unbounded homogeneous bath. A uniform electric field of strength E_0 is applied in the z direction.

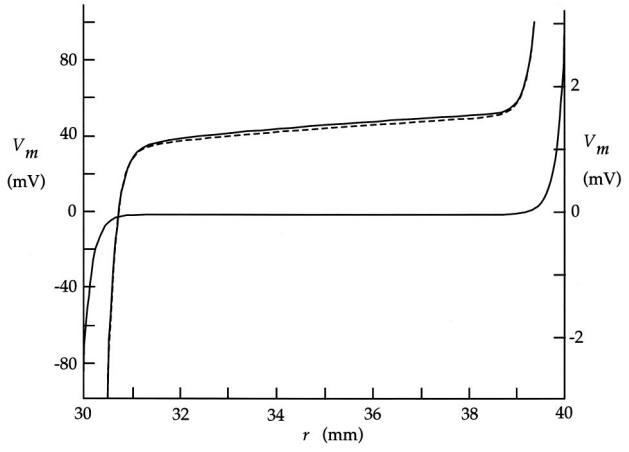

FIG. 6. The approximate analytical (solid) and exact numerical (dashed) transmembrane potentials plotted versus radial distance in a spherical heart. The endocardium corresponds to $r=30$ mm, and the epicardium to $r=40$ mm. The upper curves are plotted on the expanded voltage scale (right). $\alpha=0.25$, $e=0.75$, $\lambda=0.174$ mm, $g_T=0.0931$ S/m, $g_L=0.3726$ S/m, $g_o=2$ S/m, $g_b=0.6$ S/m, and $E_0=100$ V/m. The numerical solution uses a space step of 0.006 25mm.

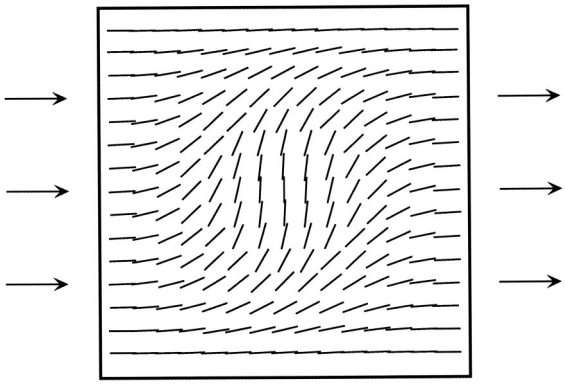

FIG. 7. The line segments indicate the fiber direction in a two-dimensional sheet of cardiac tissue, and the arrows indicate the direction of the applied electric field. A 20×20-mm region of tissue is shown, with the origin at the center.

ues. The agreement between the approximate and numerical solutions to the bidomain equations is excellent. We would expect good agreement, since the radius of curvature of the fibers ranges from 30 to 40 mm, whereas the length constant is less than 0.2 mm.

VI. EXAMPLE 4: FIBERS CURVING IN TWO DIMENSIONS

Roth and Langrill Beaudoin [4] analyzed the mechanism of tissue polarization caused by fiber curvature. They determined approximate analytical solutions to the bidomain equations that specified the distribution of polarization in a two-dimensional sheet of cardiac tissue with curving fibers. Their solutions were derived by using a perturbative expansion in powers of e. We reanalyze this problem using our iterative method.

We assume that a two-dimensional sheet of cardiac tissue has the fiber geometry shown in Fig. 7,

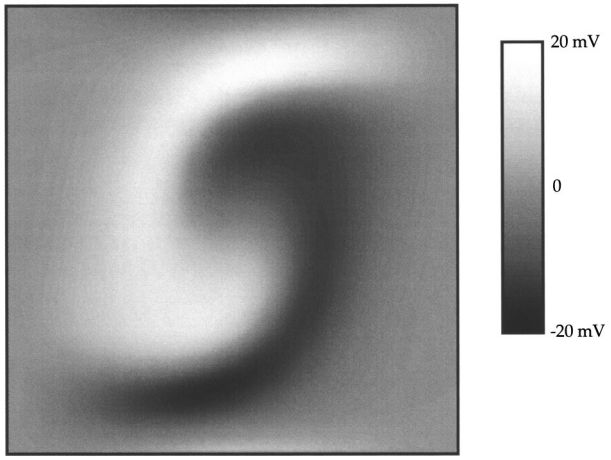

FIG. 8. The transmembrane potential produced for the fiber geometry shown in Fig. 7. $\alpha=0.25$, $e=0.75$, $\lambda=0.174$ mm, $g_T=0.0931$ S/m, $g_L=0.3726$ S/m, $D=20$ mm, and $\Delta x=\Delta y=0.2$ mm.

$$\theta(x,y) = \frac{\pi}{2}\cos^2\left(\frac{\pi x}{D}\right)\cos^2\left(\frac{\pi y}{D}\right), \tag{48}$$

where θ is the angle between the local fiber direction and the x axis. This is one of the fiber geometries used by Roth and Langrill Beaudoin [4] (see Fig. 6 of their paper). A 10-V potential difference is applied between the left and right edges of the tissue. The intracellular and extracellular conductivity tensors both have the form [4]

$$\tilde{g} = \begin{pmatrix} g_L\cos^2\theta + g_T\sin^2\theta & (g_L - g_T)\cos\ \theta \sin\ \theta \\ (g_L - g_T)\cos\ \theta \sin\ \theta & g_L\sin^2\theta + g_T\cos^2\theta \end{pmatrix}. \tag{49}$$

We substitute these conductivity tensors into Eq. (9) to get

$$(g_L\cos^2\theta + g_T\sin^2\theta)\frac{\partial^2\psi^0}{\partial x^2} + (g_L\sin^2\theta + g_T\cos^2\theta)\frac{\partial^2\psi^0}{\partial y^2} + (g_L - g_T)\begin{pmatrix} (\cos^2\theta - \sin^2\theta)\left(\frac{\partial\theta}{\partial x}\frac{\partial\psi^0}{\partial y} + \frac{\partial\theta}{\partial y}\frac{\partial\psi^0}{\partial x}\right) \\ + (2\ \sin\ \theta\ \cos\ \theta)\left(\frac{\partial^2\psi^0}{\partial x\,\partial y} + \frac{\partial\theta}{\partial y}\frac{\partial\psi^0}{\partial y} - \frac{\partial\theta}{\partial x}\frac{\partial\psi^0}{\partial x}\right) \end{pmatrix} = 0. \tag{50}$$

The first order expression for the transmembrane potential becomes

$$V_m^1 = \lambda_T^2\frac{g_L}{g_T}\frac{(1+\alpha)e}{1+\alpha-e}\begin{pmatrix} \cos^2\theta\frac{\partial^2\psi^0}{\partial x^2} + \sin^2\theta\frac{\partial^2\psi^0}{\partial y^2} + (\cos^2\theta - \sin^2\theta)\left(\frac{\partial\theta}{\partial x}\frac{\partial\psi^0}{\partial y} + \frac{\partial\theta}{\partial y}\frac{\partial\psi^0}{\partial x}\right) \\ + (2\ \sin\ \theta\ \cos\ \theta)\left(\frac{\partial^2\psi^0}{\partial x\,\partial y} + \frac{\partial\theta}{\partial y}\frac{\partial\psi^0}{\partial y} - \frac{\partial\theta}{\partial x}\frac{\partial\psi^0}{\partial x}\right) \end{pmatrix}. \tag{51}$$

We solved Eq. (50) numerically, and then evaluated the expression for V_m^1 (Fig. 8). Like in Ref. [4], we ignore the V_m^0 term because we focus on far-field effects. The solution is in good agreement with Roth and Langrill Beaudoin's numerical solution to the full bidomain equations. The iterative method in this paper appears to approximate the full solution much better than did the approximate method based on a perturbation expansion in e and the assumption of a uniform electric field.

VII. FIBERS CURVING IN THREE DIMENSIONS

In three dimensions, we need two angles in order to specify the fiber direction. A standard approach is to use the Euler angles [10]. The angle of the fibers with the z axis is specified by θ, and the angle in the x-y plane by ϕ. (Typically, three Euler angles are required to specify the orientation of an object. The third angle corresponds to rotations in the plane perpendicular to the fiber axis. We assume that the conductivity is the same in both directions perpendicular to the fiber—an assumption often but not always made [11] —so the conductivity tensor is independent of the third Euler angle.) In terms of the Euler angles, the intracellular conductivity tensor becomes

$$\tilde{g}_i = \begin{pmatrix} g_{iT}(\cos^2\phi + \sin^2\phi\ \cos^2\theta) + g_{iL}\sin^2\phi\ \sin^2\theta & (g_{iT} - g_{iL})\sin\ \phi\ \cos\ \phi\ \sin^2\theta & (g_{iL} - g_{iT})\sin\ \phi\ \cos\ \theta\ \sin\ \theta \\ (g_{iT} - g_{iL})\sin\ \phi\ \cos\ \phi\ \sin^2\theta & g_{iT}(\sin^2\phi + \cos^2\phi\ \cos^2\theta) + g_{iL}\cos^2\phi\ \sin^2\theta & (g_{iT} - g_{iL})\cos\ \phi\ \cos\ \theta\ \sin\ \theta \\ (g_{iL} - g_{iT})\sin\ \phi\ \cos\ \theta\ \sin\ \theta & (g_{iT} - g_{iL})\cos\ \phi\ \cos\ \theta\ \sin\ \theta & g_{iT}\sin^2\theta + g_{iL}\cos^2\theta \end{pmatrix}. \tag{52}$$

A similar expression exists for the extracellular conductivity tensor.

We determine the equation for V_m^1 by plugging Eq. (52) into Eq. (8) and neglecting terms containing second derivatives of V_m^1. The solution is

$$V_m^1 = \lambda^2\frac{g_L}{g_T}\frac{\alpha}{1+\alpha}\{\nabla\psi^0\cdot\tilde{D}_1\nabla\theta + \nabla\psi^0\cdot\tilde{D}_2\nabla\phi + \nabla\cdot\tilde{D}_3\nabla\psi^0\}, \tag{53}$$

where

$$\tilde{D}_1 = \begin{bmatrix} 2\ \sin\ \theta\ \cos\ \theta\ \sin^2\phi & -2\ \sin\ \theta\ \cos\ \theta\ \sin\ \phi\ \cos\ \phi & \sin\ \phi(\cos^2\theta - \sin^2\theta) \\ -2\ \sin\ \theta\ \cos\ \theta\ \sin\ \phi\ \cos\ \phi & 2\ \sin\ \theta\ \cos\ \theta\ \cos^2\ \phi & -\cos\ \phi(\cos^2\theta - \sin^2\theta) \\ \sin\ \phi(\cos^2\theta - \sin^2\theta) & -\cos\ \phi(\cos^2\theta - \sin^2\theta) & -2\ \sin\ \theta\ \cos\ \theta \end{bmatrix}, \tag{54}$$

$$\tilde{D}_3 = \begin{bmatrix} \sin^2\theta \sin^2\phi & -\sin^2\theta \sin\phi \cos\phi & \sin\phi \sin\theta \cos\theta \\ -\sin^2\theta \sin\phi \cos\phi & \sin^2\theta \cos^2\phi & -\cos\phi \sin\theta \cos\theta \\ \sin\phi \sin\theta \cos\theta & -\cos\phi \sin\theta \cos\theta & \cos^2\theta \end{bmatrix}. \quad (56)$$

The first two terms are nonzero only if the fiber direction depends on position (curving fibers). The last term is nonzero even for straight fibers if the electric field in the tissue varies with position. Our results are similar in form to those derived by Sobie *et al.* [12].

VIII. DISCUSSION

In this paper, we present an approximate, iterative scheme to solve the bidomain equations. In the problems we have examined, this method converges significantly faster than the perturbative technique examined previously [3,4]. The key element of this method is our assumption that the zeroth order contribution to the transmembrane potential decays exponentially with depth. This assumption allows us to uncouple the bidomain equations, at least in the case of equal anisotropy ratios. Another related assumption is that the length constant is much smaller than all other distances in the problem, such as the distance over which ψ^0 varies or the radius of curvature of the fibers or tissue surface. In situations in which the stimulus is applied diffusely, such as during external defibrillation, the method should be quite accurate. When the stimulus is applied locally, such as during stimulation using a small unipolar electrode [5], our method will be less useful. Furthermore, the method is not applicable when the transmembrane potential is caused by small-scale variations of conductivity, such as underlie the "saw-tooth" effect [13,14], which may play a role during defibrillation [15,16]. Finally, we assume that the fibers are parallel to the tissue surface at the surface. If this is not the case, additional boundary effects may result [17].

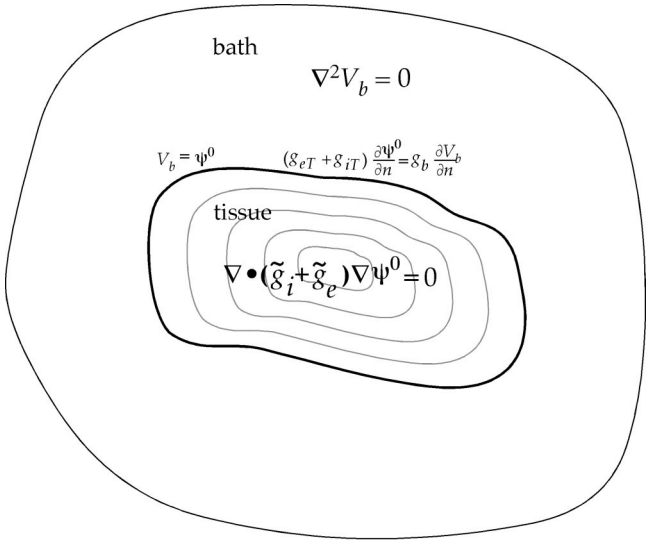

FIG. 9. A schematic diagram of the boundary value problem for ψ^0 and V_b.

We can summarize our method in Fig. 9, which outlines the boundary value problem that must be solved for ψ^0. Within the cardiac tissue $\nabla \cdot (\tilde{g}_i + \tilde{g}_e)\nabla \psi^0 = 0$, and in the bath surrounding the tissue $\nabla^2 V_b = 0$. At the tissue-bath boundary $\psi^0 = V_b$ and $g_T(\partial \psi^0 / \partial n) = g_b(\partial V_b / \partial_n)$. This boundary value problem is exactly that one would expect using a monodomain model for cardiac tissue, where the potential is given by ψ^0 and the conductivity by $\tilde{g}_i + \tilde{g}_e$. Many software packages exist for solving this type of problem, and a key feature of our method is that these packages can be applied directly to the bidomain problem. Once ψ^0 is known, we can determine the transmembrane potential by $V_m^0 = Ae^{-n/\lambda}$, with A is given by $A = \lambda(1+\alpha)(\partial \psi^0 / \partial n)$, and $V_m^1 = \lambda^2[(1+\alpha)/g_T\alpha]\nabla \cdot (\tilde{g}_i - \alpha \tilde{g}_e)\nabla \psi^0$.

Higher order terms for ψ or V_m can be computed using the iterative scheme outlined in Eqs. (7) and (8). However, in our experience only the zeroth and first order terms are required to specify the transmembrane potential accurately. The zeroth order term is often largest, but decays rapidly with depth into the tissue. The first order term accounts for "far-field" effects, and typically goes to zero in the limit of equal anisotropy ratios.

In summary, our iterative method has two advantages over a full solution to the bidomain equations. First, numerical simulations using this method are faster than solving the bidomain equations. Equations (1) and (2) represent two differential equations that need to be solved in the full bidomain calculation, whereas our problem consists of only solving one boundary value problem for ψ^0. Therefore we should experience at least a factor of two speedup. Moreover, commercial software packages that have been extensively optimized to solve boundary value problems are widely available, whereas programs to solve the bidomain equations are generally written as needed by individual researchers. Second, our method often results in analytical solutions that provide insight into the physical problem. Several of our examples illustrate this point; we could at least solve the zeroth order (equal anisotropy ratio) problem analytically, and then use that solution to determine the first order solution to the transmembrane potential.

ACKNOWLEDGMENTS

This work was supported by grants from the National Institutes of Health (Grant No. RO1 HL57207) and the American Heart Association–Midwest Affiliate.

[1] C. S. Henriquez, Crit. Rev. Biomed. Eng. **21**, 1 (1993).
[2] B. J. Roth, IEEE Trans. Biomed. Eng. **44**, 326 (1997).
[3] B. J. Roth, Phys. Rev. E **55**, 1819 (1997).
[4] B. J. Roth and D. Langrill Beaudoin, Phys. Rev. E **67**, 051925 (2003).
[5] D. C. Latimer and B. J. Roth, IEEE Trans. Biomed. Eng. **45**, 1449 (1998).
[6] N. A. Trayanova, B. J. Roth, and L. J. Malden, IEEE Trans. Biomed. Eng. **40**, 899 (1993).
[7] N. F. Otani, IEEE Trans. Biomed. Eng. **51**, 401 (2004).
[8] B. J. Roth, Ann. Biomed. Eng. **19**, 669 (1991).
[9] W. Krassowska and J. C. Neu, IEEE Trans. Biomed. Eng. **41**, 143 (1994).
[10] H. Goldstein, *Classical Mechanics*, 2nd ed. (Addison-Wesley, Reading, MA, 1980).
[11] I. J. LeGrice, B. H. Smaill, L. Z. Chai, S. G. Edgar, J. B. Gavin, and P. J. Hunter, Am. J. Physiol. **269**, H571 (1995).
[12] E. A. Sobie, R. C. Susil, and L. Tung, Biophys. J. **73**, 1410 (1997).
[13] R. Plonsey and R. C. Barr, Med. Biol. Eng. Comput. **24**, 130 (1986).
[14] W. Krassowska, T. C. Pilkington, and R. E. Ideker, IEEE Trans. Biomed. Eng. **34**, 555 (1987).
[15] J. P. Keener, J. Theor. Biol. **178**, 313 (1996).
[16] V. I. Krinsky and A. Pumir, Chaos **8**, 188 (1998).
[17] B. J. Roth, Med. Biol. Eng. Comput. **37**, 523 (1999).